

Large Area Three-Dimensional Photonic Crystal Membranes: Single-Run Fabrication and Applications with Embedded Planar Defects

Bingdong Chang,* Chen Zhou, Abebe Tilahun Tarekegne, Yuanqing Yang, Ding Zhao, Flemming Jensen, Jörg Hübner, and Henri Jansen


Three-dimensional photonic crystals (3D PhCs) enable light manipulations in all three spatial dimensions, however, real world applications are still faced with challenges in fabrication. Here, a facile fabrication strategy for 3D silicon PhCs with a simple cubic (SC) lattice structure is presented, which exhibits a complete photonic bandgap at near-infrared wavelengths of around 1100 nm. The fabrication process is composed of standard deep ultra-violet stepper lithography, followed by a single-run modified plasma etch process. By applying a direct dry etch release step at the end of the 3D structural etch process, the fabricated 3D PhCs can be released and transferred in the form of a membrane onto other substrates such as glass, polymers, or even substrates with engineered surface. The thickness of the demonstrated membranes is around 2 μm and the size can be up to a few millimeters. A high reflectivity is observed at the stop band frequency, and a planar defect is introduced during the etching process resulting in an optical resonance mode with a small linewidth of around 30 nm. The structure constitutes an optical bandpass filter and can be used as a sensor for organic solvents.

1. Introduction

Three dimensional photonic crystals (3D PhCs), with periodic modulations of dielectric constants in three dimensions, possess a modified dispersion relation and a photonic bandgap

B. Chang, Dr. D. Zhao, Prof. F. Jensen, Prof. J. Hübner, Prof. H. Jansen
DTU Danchip
Technical University of Denmark
Kongens Lyngby 2800, Denmark
E-mail: bincha@dtu.dk

C. Zhou
DTU Nanotech
Technical University of Denmark
Kongens Lyngby 2800, Denmark
Dr. A. T. Tarekegne
DTU Fotonik
Technical University of Denmark
Kongens Lyngby 2800, Denmark
Dr. Y. Yang
SDU Nano Optics
University of Southern Denmark
Odense 5230, Denmark

 The ORCID identification number(s) for the author(s) of this article can be found under <https://doi.org/10.1002/adom.201801176>.

DOI: 10.1002/adom.201801176

(PBG). This results in a range of wavelength, where electromagnetic propagating modes are forbidden, and is an optical analog to the electronic bandgap structures of atomic lattices. By incorporating defects with 3D PhCs, a localized optical resonance mode can be realized in the defect region, and more advanced functionalities can be demonstrated. PhCs with lower dimensions have already been widely used in various fields such as optical waveguides and sensors. However, 3D PhCs, which enable light manipulations in full three spatial dimensions, are still faced with fabrication challenges. A lot of effort has been invested in previous studies, and various fabrication methods have been proposed, most of which are limited by fabrication complexity and cost. The classical 3D PhC configurations such as woodpile structures^[1,2] and inverse opal

structures^[3,4] enable a large bandgap ratio (bandgap width over mid gap position) and flexibilities to manipulate photons with embedded cavities.^[5–7] However, these bottom-up strategies require multiple complex fabrication steps and are not suitable for large scale production. Some top-down methods have been proposed to fabricate 3D PhC in a convenient manner, but they do need nonstandard fabrication instruments.^[8–12] Fabrication of 3D PhC in a large scale can be realized by plasma etching^[13] or modulated electrochemical etching.^[14] However, there is still a need for feasible fabrication methods for large scale 3D PhCs and embedded cavities.

The idea to fabricate large scale 3D PhCs simply by using the plasma etching was first proposed by Venkataraman et al.^[15] A similar study was later reported by Vlad et al.,^[13] both of them made use of the so called “scallop,” which are generated during the Bosch process etch cycles and can give a ripple-like sidewall profile to create the necessary modulation of the refractive index. Thus, a 2D pattern from a traditional lithography can be transferred into 3D PhC in a top-down manner. This method has the advantage of high fabrication efficiency and low cost. However, there are some technical limitations. First, the size and the shape of the scallops are difficult to control precisely, since the Bosch process is limited intrinsically by ion angular distribution (IAD) and effects such as aspect ratio dependent etching (ARDE).^[16,17] All of them will influence not only the

etch rate, but also the sidewall profile along the etch depth in the silicon, generating nonuniformities affecting the periodicity of the structure. Second, the simple cubic (SC) lattice type of 3D PhCs have a relatively small bandgap ratio of less than 10%,^[18] thus geometric distortions or nonuniformity of lattices can close the bandgap in certain directions of Brillouin zone, and the stop band can only exhibit in certain angles of incidence (referred to as pseudo PBGs^[19]). Third, to achieve a complete bandgap that is incident angle independent with a high attenuation rate of around 20 dB in mid gap position, a large contrast of refractive index is necessary, thus a strong structural shape modulation of the scallops is necessary, which will at the same time reduce the mechanical stability of the structures.^[13,15] All of the disadvantages mentioned above will limit the capabilities and flexibilities of the fabricated structures. Besides, the total number of repeated layers will be limited and the precise introduction of defects will be difficult, ultimately limiting the functionalities of the fabricated structures.

Here, we report a novel multistep one-run fabrication process for 3D PhCs with a SC configuration. The 2D patterns were defined with standard deep ultra-violet (DUV) stepper lithography, and a modified DREM (deposit, remove, etch, multistep) etch process was then performed to transfer the patterns into silicon in such a manner that a 3D shaped structure is realized.^[20,21] Compared with the scallops created directly by Bosch process,^[13] a large refractive index contrast can be realized due to the strongly modulated etch profile. The fabricated 3D PhCs also show excellent mechanical properties, which enable the structures to be lifted off the substrate and be transferred as a membrane onto other substrates, or to be infiltrated by polymers. Moreover, by infiltrating the air voids in 3D PhC membranes with polymer, a self-supported flexible hybrid film can be fabricated, with 3D silicon structure embedded, while the features of bandgap still preserved. To enable optical functionalities of the fabricated 3D PhCs, planar defects are introduced directly during the modified etch process, which results in a resonance mode coupled to PBG at a wavelength of around 1100 nm, with a linewidth of around 30 nm. We have demonstrated that the fabricated 3D PhC membrane with embedded planar cavity can be used as a sensor for organic solvents with a good sensitivity of around 400 nm RIU⁻¹ (RIU, refractive index unit). By transferring the 3D PhC membranes onto n-doped black silicon, the near-infrared (NIR) photoluminescence (PL) of the black silicon^[22] could be filtered efficiently with an attenuation ratio of around 20 dB.

2. Results and Discussion

2.1. Fabrication Process

The time multiplexed Bosch process is a standard plasma etching technique in conventional complementary metal-oxide semiconductor (CMOS) micro- and nanofabrication industries. By applying a passivation step with inhibitors (such as CF₂ from C₄F₈), some ion bombardment using a radiofrequency platen power source, and a step with isotropic etching species (such as F from SF₆) sequentially, the sidewall can be protected, and the etch process can proceed in an anisotropic manner.

Since the etch step with SF₆ is isotropic, the sidewall has normally a “rippled” profile with shape modulations known as scallops, which has been suggested before for fabrication of 3D PhCs.^[13,15] In order to have a large modulation of the etch profile, the amplitude of the scallop needs to be maximized. This, however, might delaminate and destroy the structures. To have a better profile control of the structures and more flexibility in fabrication, we applied a modified DREM etch process as introduced in our previous studies.^[20,21] A schematic view to compare the Bosch process and the modified DREM process can be seen in Figures S1 and S2 in the Supporting Information. We will show later that this technique enables a better mechanical stability of the fabricated structures and a large modulation of the refractive index. More importantly, planar cavities can be embedded conveniently and are easily introduced by programming the etching sequence during the fabrication process. The fabricated 3D PhCs were then released into freestanding membranes by a final dry release step. The details of the fabrication process will be introduced below.

In a DREM process, the bottom removal of the passivation layer and the isotropic etch of silicon are fully decoupled, thus the size of scallops can be minimized, at the same time, a straight profile can be achieved and the sidewall can be well protected from ion bombardment.^[20] A process flow of the modified DREM process^[21] is shown in **Figure 1a**. First, DUV stepper lithography was performed to define the patterns (see **Figure 1a1**). Second, 5 DREM cycles were applied to etch into silicon and create straight hole structures (see **Figure 1a2**). Each scallop has the size of around 20 nm, which is much smaller than the scallop sizes from the traditional Bosch process, which is typically around a few hundred nanometers.^[13,15] In the next step, an isotropic etch was performed with SF₆ gas without platen power to maximize the isotropicity (**Figure 1a3**), thus generating a large shape modulation. By repeating these two steps subsequently, 3D periodic structures have been fabricated. Since the structures are strengthened by the anisotropic part of the etch profile, the sequences can be repeated for at least eight times (limited by the thickness of photoresist), and the fabricated 3D periodic structures can be released from silicon substrate by a final isotropic etch step with a longer etch time not resulting into structural collapse (**Figure 1a4**). The fabrication process is CMOS compatible and based on the standard fabrication techniques. The etch process takes only a few minutes, and the sequence is easy to be programmed, so that the period and the size of void can be tuned in a reasonable wide range.

The total thickness of the fabricated membranes is around 2 μm, and area can be several square millimeters. In **Figure 1b**, we can see that the fabricated 3D PhCs can be peeled off by tweezers and transferred to a piece of quartz wafer (**Figure 1b4**). The membranes can also be infiltrated by polymer, thus a flexible film can be fabricated with 3D PhCs embedded (**Figure 1b5**) (for membranes with even larger area, other transfer methods might be necessary, since the membranes will break at the contact point with tweezers). It should be noticed that the 3D PhCs membranes are porous and can be infiltrated with liquids, e.g., polymer, thus the silicon structures could be supported by the soft polymer, and a good flexibility

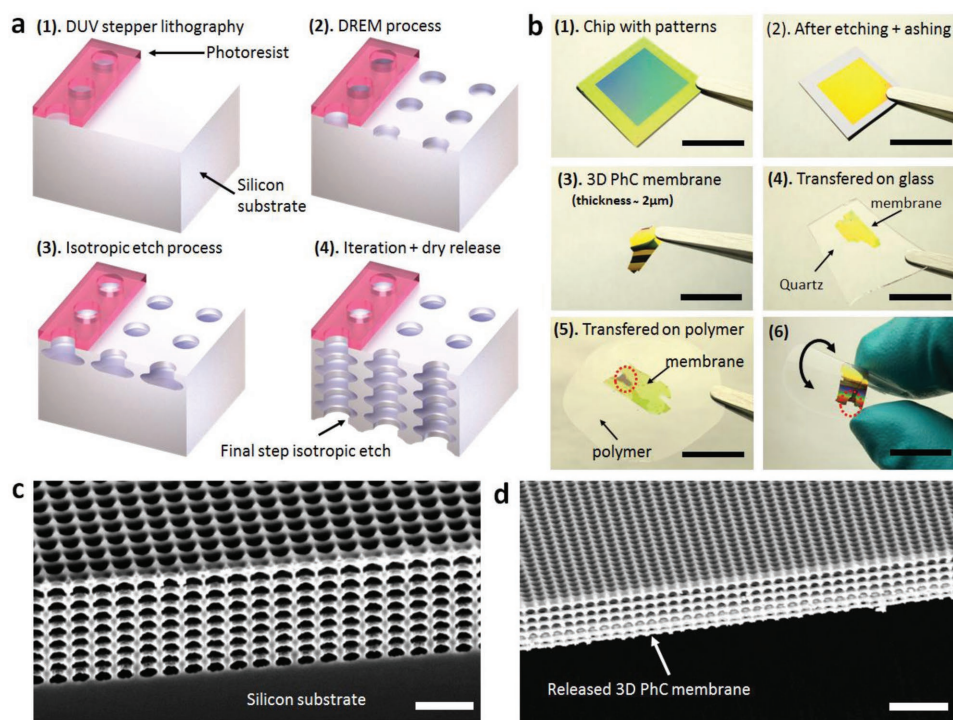


Figure 1. a) Fabrication process of 3D photonic crystal membranes, which includes pattern definition with DUV stepper lithography (1), iterative DREM process (2) and isotropic etch (3), and final step of dry release to detach the membrane from silicon substrate (4). b) Photographic illustration of the process flow, which shows the chip with pattern area of $1 \times 1 \text{ cm}^2$ (1), chips after etching process and plasma ashing to remove the photoresist (2), freestanding 3D photonic crystal membranes (3), membranes transferred on a piece of quartz (4), membranes infiltrated and transferred on a piece of flexible polymer plate (5), and the sample from (5) being bent (6), scale bars 1 cm. c) SEM image of 3D PhCs with eight periods before last step of dry release, scale bar $1 \mu\text{m}$. d) SEM image of freestanding 3D photonic crystal membranes with six periods after dry release, scale bar $2 \mu\text{m}$.

can be achieved resulting in a polymer membrane integrated with a 3D PhCs membrane (Figure 1b6), to fabricate flexible photonic devices. The scanning electron microscopy (SEM) images show the 3D PhCs fabricated on the silicon substrate before final release (Figure 1c) and in the membrane form (Figure 1d). After peeling off from silicon substrate, the structure of membrane remains intact.

There are several technical challenges that we had to address during the fabrication process. The first is that the silicon-to-air volume ratio during the isotropic etch step can reduce to less than 10%, thus a proper isotropic etch time should be chosen. Otherwise, the layers can delaminate from each other (as shown in Figure S3, Supporting Information). Another effect that needs to be considered is the ARDE, which is especially prominent for hole-like structures, due to ion shadowing^[16] and the poor depletion of etching reactants in a confined space, and the etch rate can drop significantly when the aspect ratio increases. When the etch process goes deeper into the structures, the etch rate will be aspect ratio dependent and the etch process will slow down gradually, thus the periodicity of the structures will be compromised. In our process, both the etch step during DREM process and the isotropic etch step are ramped along with the process time (a technique we call parameter ramping), so the possible shape nonuniformity is compensated and precise periodicity can be achieved (a comparison of profiles with and without parameter ramping is shown in Figure S4, Supporting Information).

2.2. Characterization of 3D Photonic Crystal Membranes

The fabricated 3D PhCs membranes have a well-defined SC structure as shown in Figure 2a, in which a unit cell is also labeled. The width a of the cubic cell is 400 nm, and the diameter d of the lithography patterns is around 250 nm. A void with diameter larger than 400 nm is created during the isotropic etch step, such that each unit cell is connected with its neighboring cells, resulting in a strong shape modulation. Based on the volume proportion of silicon in different layers, a large refractive index contrast of around 1.53 is estimated along the direction of the holes. In some cases, silicon single crystalline structures could be damaged during the plasma etching process due to UV irradiations or ion bombardments, thus the refractive index, especially the absorption coefficient, could change. To rule out this effect, X-ray diffraction (XRD) measurements were performed for both a silicon dummy wafer and a 3D PhC membrane on top of glass; the spectra are shown in Figure 2b. We can clearly see the sharp diffraction peak of (400) silicon crystalline plane at around 69.24° , which suggest a good single crystalline quality after plasma etching process (the peak with lower intensity at around 61° corresponds to the Cu $K\beta$ radiation source). We measured the reflection spectrum of fabricated 3D PhC membranes on glass substrate at incident angles of 7.5° , 15° , and 30° with a goniometer stage and broadband optical spectrometer as shown in Figure 2c. A strong reflection peak at $\lambda = 1100 \text{ nm}$ is present, which fits well with

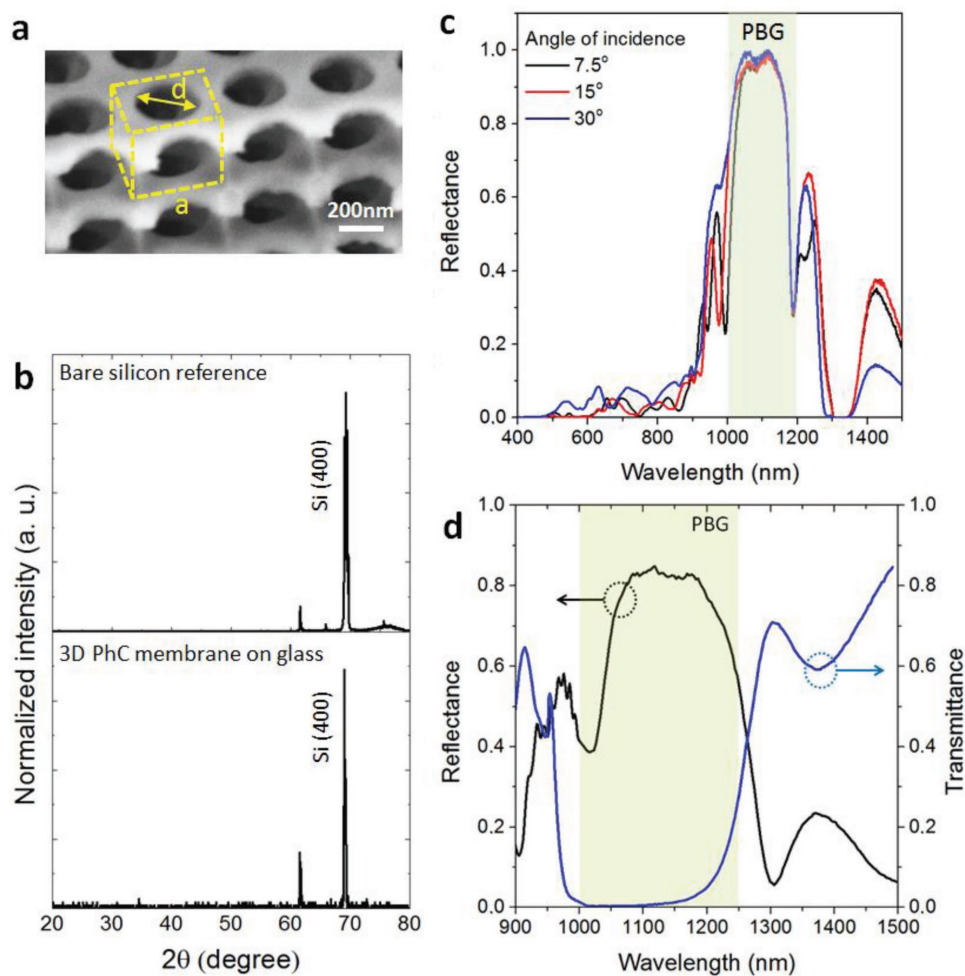


Figure 2. a) SEM image of fabricated 3D PhC structures, in which a unit cell is labeled with yellow lines; b) XRD measurements of a bare silicon wafer and 3D PhC membranes on top of glass substrate; c) reflection spectrum of 3D PhC membranes on glass measured with three different angles of incidence using goniometer stage and an optical spectrometer; d) reflection and transmission spectrum of 3D PhC membranes on glass measured by ellipsometry (incident angle of 45° for reflection measurement).

the band-edge position as in previous studies for 3D PhCs with SC geometry.^[14] The gap to mid gap ratio $\Delta\lambda/\lambda = 18\%$. Reflection and transmission spectrum were also measured with an ellipsometer as shown in Figure 2d, displaying the low transmittance in the PBG region (the reflectance was measured with 45° incident angle, while the transmittance was measured with 0° incident angle).

Since the fabricated 3D PhC membranes have the advantage of large surface area, the reflectance spectrum can be easily measured by a compact spectroscopic ellipsometer without focused probes. To prove the fabricated 3D PhC membranes have complete PBG, the reflectance spectrum was measured with varying incident angles θ in a large range from 45° to 75°, and the incoming angle φ as 0° and 45°. To demonstrate both sides of the membranes have the same optical properties, we also measured the reflection spectrum from both top side and bottom side of the 3D PhCs membranes on top of glass, as shown in Figure 3a. The measured spectrum agrees with the measurement made using a standard spectrometer in Figure 2c, showing a significant reflectance peak in the

bandgap region. The band diagram is also calculated by finite-difference time-domain (FDTD) simulation (Figure S5, Supporting Information), suggesting a complete bandgap, and the position of measured reflectance peak fits nicely with the calculated bandgap position. The reflection spectra along the (110) plane for 3D PhC membranes on different substrates are compared in Figure 3b. The reflection maxima and the band-edge position coincide well with each other for 3D PhC membranes on glass and on silicon, while for the membranes infiltrated with a low refractive index polymer (Efron, refractive index $n = 1.404$ at $\lambda = 852$ nm after curing by UV light), the band edge was redshifted by around 80 nm, which is expected. Since the void in the structures is replaced by polymer with a higher refractive index of around 1.3, the mean refractive index will increase and position of band edge will shift to a lower frequency range. Besides, the SC structures might be distorted due to the strain introduced by polymer infiltration, thus the reflection spectrum might be altered compared with a free standing membrane on glass or silicon. When increasing the number of periods for 3D PhCs from four layers to eight layers, we could

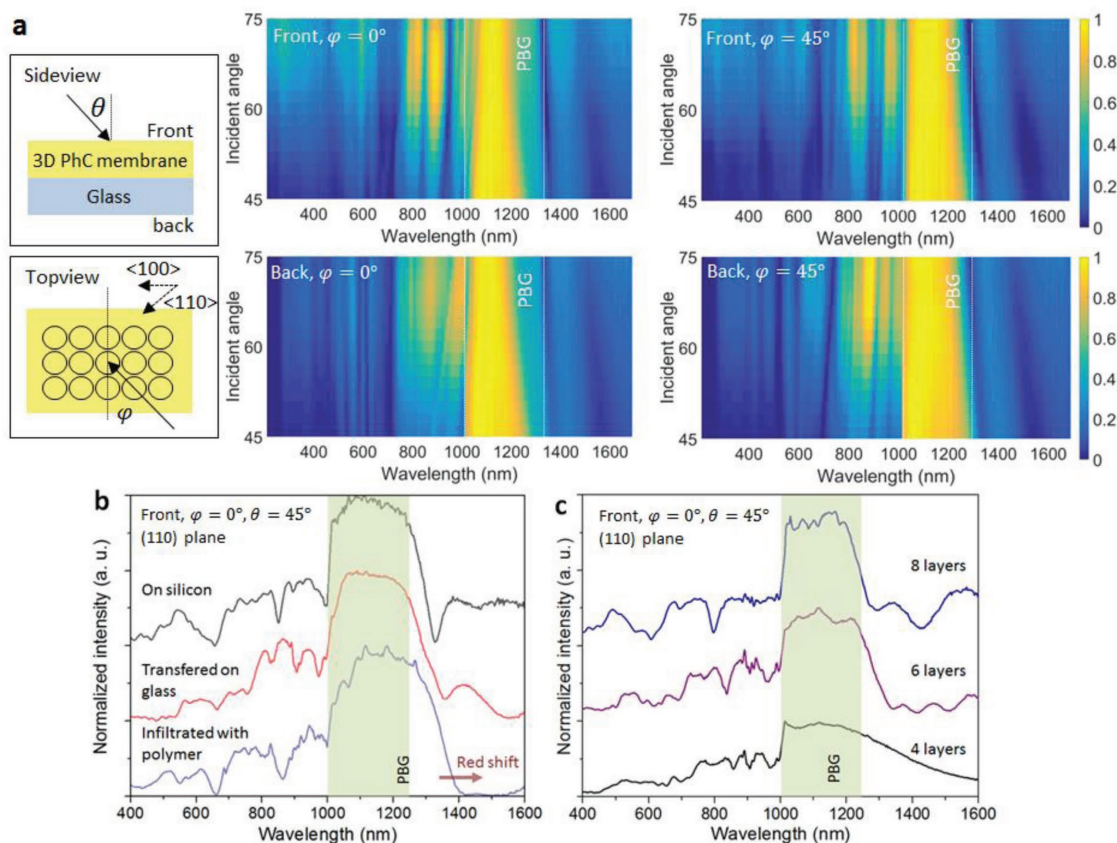


Figure 3. Reflection spectra measured by ellipsometry. a) A schematic view of the 3D PhC membranes on glass substrate, and measured reflection spectrum from both the front and back side of the sample with different incident angles, which show a clear bandgap region at around 1100 nm; b) reflection spectrums of 3D PhC membrane on different kinds substrates: silicon, glass, and polymer; c) reflection spectrums with different numbers of repeating layers of 3D PhC membranes on glass substrate.

clearly see the development of the PBG, as the reflection in mid gap position increases by around 60%.

As already shown in Figure 1b5, the fabricated 3D PhC membranes could be easily infiltrated by polymer, and the integrated 3D PhC membranes on the polymer possess mechanical flexibility and can be bent in a large scale without collapse, which implies the potential for flexible and wearable photonic devices. It should also be noticed that shear strain can be introduced in 3D PhC structures when the polymer membrane is bend, thus the SC geometry will be distorted as shown in Figure 4a, where the shear strain can be as large as 0.48. The band structures will also be modified, thus realizing tunable and flexible photonic devices that can be compatible with biological systems,^[23,24] which will be interesting to investigate, but are not within the scope of this article. Apart from polymers, some high refractive index materials could also be infiltrated and coated conformally on the 3D PhC membranes by atomic layer deposition (ALD) method. Figure 4b is a 3D PhC membrane coated with titanium dioxide (TiO_2) on a glass as substrate. The energy dispersive X-ray (EDX) mapping shows a uniform coating of TiO_2 on the membrane. When the thickness of TiO_2 increases from 10 to 15 nm, the band edge is redshifted due to the increased average refractive index, while the reflection intensity decreases significantly, which is supposed to be caused by the increased volume ratio of high refractive index materials, thus the complete PBG

closes. However, it should be mentioned that in order to achieve a better optical performance of fabricated PhCs, it is an efficient method to coat 3D PhC structures with materials with better thermal or optical properties,^[25] or creating inverse structures and replicas with other materials.^[26,27] By carefully choosing the dimensions of the 3D PhC membranes, it should be possible to make inverse 3D PhCs with other materials, which is a subject of future study.

2.3. Embedded Planar Cavities and Applications

To enable the functionalities of 3D PhCs for the purpose of light manipulation, defects are introduced into the structures, such as planar cavities, single point defect, or even complex 3D waveguides which can guide the light in three dimensions.^[28] Planar defects have been studied mostly for different configurations of 3D PhC.^[29–31] Here, we will show how a planar cavity could be introduced into our 3D PhC membranes for different applications. Figure 5a is a free standing 3D PhC membrane with six periods; the cross section shows a good size uniformity for six layers. Figure 5b is a free standing 3D PhC membrane with seven layers, with a defect layer embedded in the middle with a thickness of around 300 nm. The planar defect was introduced simply by increasing the number of DREM cycles

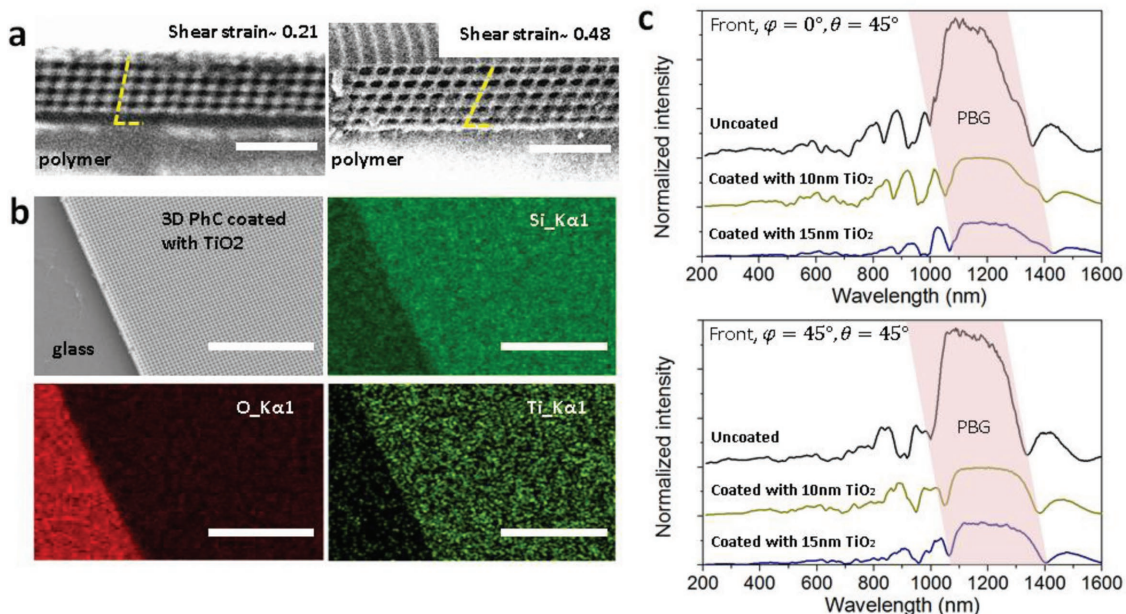


Figure 4. a) 3D PhC membranes infiltrated with polymer under shear stress (scale bars 2 μm); b) SEM image and EDX mapping of 3D PhC membrane coated with 15 nm TiO_2 by ALD (scale bars 10 μm); c) reflection spectra of 3D PhC membranes coated with different thickness of TiO_2 , with glass as substrate.

for the fourth layer, while the other layers remain in good size uniformity. The reflection spectrums for 3D PhC membranes on glass substrate with and without embedded planar defects are shown in Figure 5c,d. Since photonic states are introduced

in the stop band by the planar defects, a resonance could be clearly seen in the PBG region, which should otherwise be free from photon propagations. The resonance has a linewidth of around 30 nm, and can be observed with incident angles from

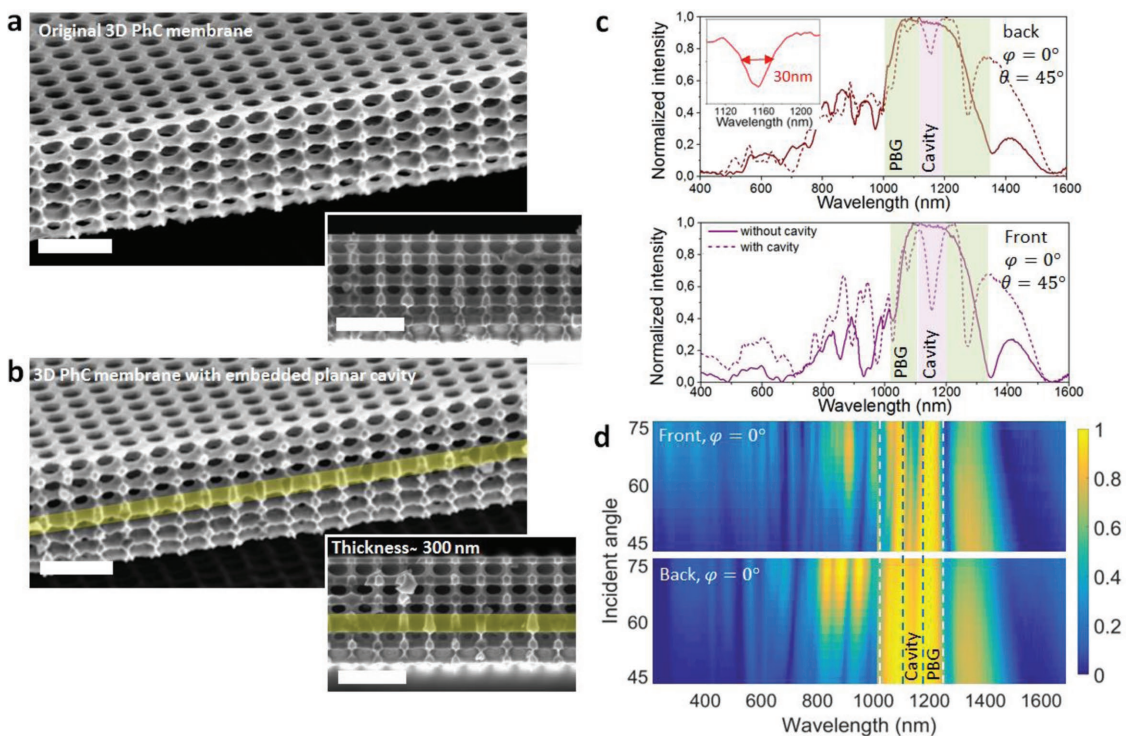


Figure 5. 3D PhC membranes with embedded planar cavity. SEM image of freestanding 3D PhC membranes a) without cavity and b) with planar cavity, scale bars 1 μm ; c) the comparison of reflection spectra, which shows a cavity resonance mode in the PBG with a linewidth of 30 nm; d) the reflection spectrum of a 3D PhC membrane (with cavity) on glass, with different incident angles.

45° to 75° from both the top side and the bottom side of the membranes. It should be addressed that there are several resonance dips near the bandgap position on the spectra. This is possibly due to the high volume ratio of silicon dielectric defect, which can host multiple localized resonance modes,^[32,33] while for silica planar defects^[30,31] or air defects,^[7] only a single resonance dip can be observed, which is generated by the basic dipole resonance state or monopole state. To further increase the quality factor of the planar cavity resonance mode, the effective cavity length should be increased, e.g., by increasing the number of repeated defect-free layers to achieve a better confinement of states in the cavity region. A thermal annealing process is also promising to reduce the roughness on structure surfaces, thus less scattering loss is generated and the quality factor can be increased for a sharper resonance dip.

The porous structure of fabricated 3D PhC membranes enables solvents and gases to easily infiltrate, thus the refractive index can be tuned in a controllable manner. Here, we applied ethanol with different concentrations (in deionized water) onto the 3D PhC membrane with glass as the substrate. The reflection spectrum was then measured using an ellipsometer

at an incident angle of 45°. A redshift could be observed both for the band edge of the reflection peak and the resonance mode of the planar cavity as shown in Figure 6a. This can be explained as the electromagnetic confinement in the silicon cavity region started to leak inside the surrounding medium of the solvent with a higher refractive index than air, and both the air band and dielectric band will be suppressed to a lower frequency level. The correspondence between the center wavelength of the resonance mode and the refractive index of infiltrated solvent is recorded and shown in Figure 6b, which suggested a sensitivity of around 397 nm RIU⁻¹. This is comparable with the result from silk inverse opal structures.^[34,35] After each measurement, the sample can be soft baked to let the solvents fully evaporate from the porous structures, thus making it suitable for multiple usage for sensing gases or solvents.

We also transferred the fabricated 3D PhC membranes onto substrates with engineered surfaces as shown in Figure 6c (more SEM images with details is in Figure S6, Supporting Information), which can be difficult with traditional 3D PhC structures. The substrates we used were highly-doped black silicon created by Bosch etch process, which is known to exhibit room

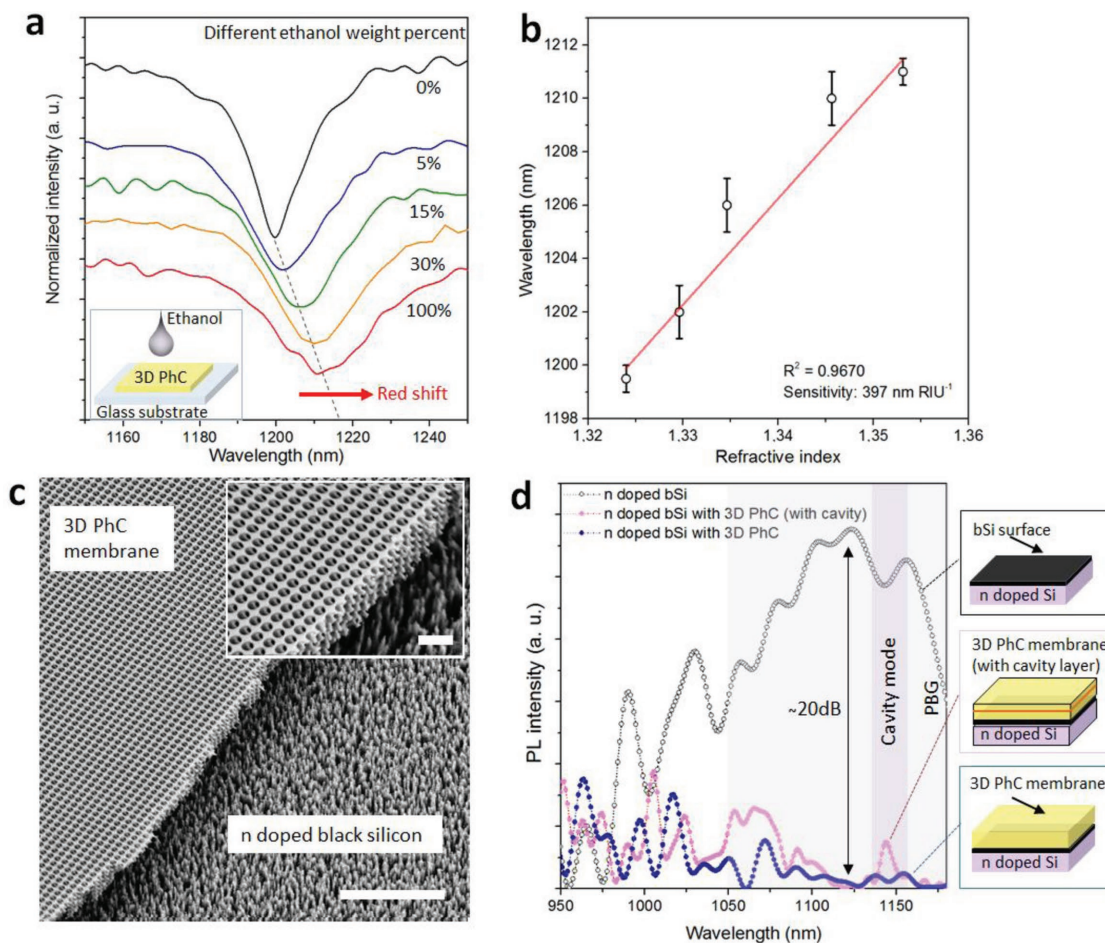


Figure 6. Applications of 3D PhC membranes with embedded planar cavities. a) The redshift of the resonance peak when ethanol solution with different concentrations (in deionized water) is applied on the membrane. b) The relation between the resonance peak wavelength and refractive index of ethanol solutions. c) SEM images of transferred 3D PhC membranes on n-doped black silicon substrate, scale bars 5 μm , with a close up view in the inset, scale bars 1 μm ; d) the PL intensity with a black silicon reference sample, black silicon sample covered with 3D PhC membranes, and black silicon sample covered with 3D PhC membrane with an embedded planar cavity.

temperature band-edge PL NIR wavelengths.^[22] Photoexcitation was performed with a 532 nm continuous wave (CW) laser, allowing detection of the PL signals with an InGaAs detector. When the surface of the black silicon was covered with a 3D photonic crystal membrane (with six periods, thickness of around 2 μm), the PL intensity in the PBG region was suppressed with an attenuation rate of around 20 dB as shown in Figure 6d, while the PL signal could still be detected in the wavelength away from PBG region. When a membrane with a planar cavity was transferred on top of black silicon, the PL intensity in the bandgap region was still low, but had a noticeable peak at the wavelength of cavity resonance mode, which in this case acted as an optical bandpass filter. However, due to the optical absorption of the silicon material at 532 nm, the PL intensity at resonance wavelength was also reduced. Nevertheless, this demonstrates the possibility to apply the 3D photonic crystal membranes as an optical bandpass filter that is adaptable for different substrates.

3. Conclusions

In this work, we have demonstrated a one-step fabrication process for 3D photonic crystal membranes. The fabricated membranes have a thickness of around 2 μm with excellent mechanical stability. Reflectance spectra were recorded at different angles of incidence from 7.5° to 75°, suggesting a complete PBG structure with a peak reflection at around 1100 nm. We transferred the fabricated membranes (manually, using tweezers) onto different substrates such as glass or black silicon surfaces. A soft 3D PhC membrane could be achieved by infiltrating the structures with polymer. In addition, we demonstrated that a planar defect can be conveniently introduced into the 3D PhC structures during the fabrication process, giving an optical resonance mode coupled with the stop band. The narrow resonance peak of around 30 nm linewidth can be used for sensing the concentrations of organic solvents. The PL from black silicon could be filtered effectively by 3D PhC membranes with the incorporated planar defect. Our study provides a convenient strategy for large scale fabrication of flexible 3D PhC membrane structures with the feasibility to introduce planar cavities and possibilities for integration on different photonic devices. We have shown the feasibility of some practical applications within optics and chemical sensing. Other obvious application areas include biological sensors (e.g., in connection with bacteria/cell growth) as well as optical communications and lasers. The whole fabrication process is performed by standard fabrication technologies in the semiconductor industry and is CMOS compatible.

4. Experimental Section

DUV Stepper Lithography: Silicon wafers (150 mm, n-doped, <100> orientation) were first coated with 65 nm thick bottom antireflective coating (BARC, DUV42s-6, Brewer Science) layer in a spin coating system (Gamma 2M, Süss). Afterwards, a 360 nm thick DUV resist (JSR KRF M230Y, JSR-Micro) was coated on top of the BARC layer. Patterns were exposed with a DUV stepper lithography system (FPA-3000EX4, Canon), which was equipped with a 248 nm KrF excimer laser (intensity 280 mW cm⁻², dose 21 mJ cm⁻², and focus depth 0.17 μm). Finally, the samples were developed in AZ726 (AZ Electronic Materials).

Plasma Etching: The plasma etching process was performed in a dual source inductively coupled plasma (ICP) etching system (DRIE Pegasus, SPTS). Samples with patterns after lithography were diced manually into pieces (around 1.5 cm \times 1.5 cm) and attached on an alumina coated silicon carrier wafer using a small amount of Fomblin oil (Solvay Solexis S.P.A.), a kind of chemically inert perfluoropolyether vacuum oil with good thermal conductivity. The alumina was coated by a R200 ALD system (Picosun), the thickness was measured to be 100 nm.

Transfer of 3D PhC Membranes: 3D PhC membranes were released from bulk silicon substrate during etch process, which could be easily peeled off using tweezers and then manually transferred onto glass substrates. To transfer and infiltrate the 3D PhC membranes with polymer, Efron PC-404 (Lucantix, South Korean) was first applied onto the membranes (with a silicon wafer treated with an anti-stiction layer of 1H,1H,2H,2H-Perfluorodecyltrichlorosilane as a substrate), and then cured under UV lamp for 5 min (13.5 mW cm⁻² at 365 nm); afterwards, the hardened resist was released together with 3D PhC membranes from the silicon wafer.

Characterizations of Structures: The thickness of the BARC layer and resist were measured by a spectroscopic ellipsometer (Vase, J.A. Woollam Co., Inc.). SEM (Supra V60, Zeiss) images were taken to characterize the dimension and morphology of the structures. Crystallographic information of fabricated samples was collected with a high-resolution X-ray diffractometer system (SmartLab, Rigaku), which was equipped with a Cu K α radiation source (1.54 Å).

Characterizations of Optical Properties: The reflection and transmission spectrums were measured by a spectroscopic ellipsometer (Vase, J.A. Woollam Co., Inc.) with incidence angle from 45° to 75°, the spot size was 1 mm \times 1 mm, and the wavelength ranges from 200 to 1600 nm. The reference sample was a silicon wafer deposited with 25 nm SiO₂. To confirm the result of measurements over broader angles of incidence, the reflection spectrum was also measured at incident angles of 7.5°, 15°, and 30° using a goniometer stage (Gon360 from Instrument Systems) and a broadband optical spectrometer (Spectro320 from Instrument Systems) with a wavelength range from 400 to 1600 nm. Reflectance measurement of a silver-coated mirror was used as a reference. A broadband light from a Xenon lamp (HPX2000 from Ocean Optics) was used as a source for the reflectance measurements.

PL Measurement: The PL measurement was carried out on RPM2000 Rapid Photoluminescence Mapper (Nanometrics). The black silicon reference samples were fabricated with a Bosch etch process from an n-doped silicon wafer (antimony doped, resistivity <0.25 Ohm cm, doping concentration around 2×10^{28} cm⁻³). The samples were then cleaned with plasma ashing (400 sccm O₂, 70 sccm N₂, with coil power of 1000 W). A CW laser source of 532 nm (with the power of 7.11 mW) and an InGaAs detector were used.

Supporting Information

Supporting Information is available from the Wiley Online Library or from the author.

Acknowledgements

The authors would like to thank DTU Danchip staff for instrument support. Especially, the authors thank Elena Khomtchenko and Dr. Matthias Keil for support with DUV stepper lithography, Dr. Rebecca Ettlinger for XRD measurement, Roy Cork and Martin Nørvang Kristensen for technical support with DRIE processes, and Jonas Michael-Lindhard for fruitful discussions. D. Zhao is grateful for financial support from the European Union's Horizon 2020 research and innovation program under the Marie Skłodowska-Curie grant agreement No. 713683.

Conflict of Interest

The authors declare no conflict of interest.

Keywords

3D photonic crystals, DREM process, planar cavities, plasma etching, silicon

Received: August 29, 2018

Revised: October 21, 2018

Published online: December 3, 2018

-
- [1] S. Y. Lin, J. G. Fleming, D. L. Hetherington, B. K. Smith, R. Biswas, K. M. Ho, M. M. Sigalas, W. Zubrzycki, S. R. Kurtz, J. Bur, *Nature* **1998**, 394, 251.
- [2] S. Noda, K. Tomoda, N. Yamamoto, A. Chutinan, *Science* **2000**, 289, 604.
- [3] Y. A. Vlasov, X. Z. Bo, J. C. Sturm, D. J. Norris, *Nature* **2001**, 414, 289.
- [4] A. Blanco, E. Chomski, S. Grabtchak, M. Ibisate, S. John, S. W. Leonard, C. Lopez, F. Meseguer, H. Miguez, J. P. Mondia, G. A. Ozin, O. Toader, H. M. van Driel, *Nature* **2000**, 405, 437.
- [5] K. Ishizaki, M. Koumura, K. Suzuki, K. Gondaira, S. Noda, *Nat. Photonics* **2013**, 7, 133.
- [6] K. Ishizaki, S. Noda, *Nature* **2009**, 460, 367.
- [7] S. A. Rinne, F. García-Santamaría, P. V. Braun, *Nat. Photonics* **2008**, 2, 52.
- [8] S. Takahashi, K. Suzuki, M. Okano, M. Imada, T. Nakamori, Y. Ota, K. Ishizaki, S. Noda, *Nat. Mater.* **2009**, 8, 721.
- [9] M. Campbell, D. N. Sharp, M. T. Harrison, R. G. Denning, A. J. Turberfield, *Nature* **2000**, 404, 53.
- [10] X. Wang, J. F. Xu, H. M. Su, Z. H. Zeng, Y. L. Chen, H. Z. Wang, *Appl. Phys. Lett.* **2003**, 82, 2212.
- [11] J. M. Van den Broek, L. A. Woldering, R. W. Tjerkstra, F. B. Segerink, I. D. Setija, W. L. Vos, *Adv. Funct. Mater.* **2012**, 22, 25.
- [12] C. C. Cheng, V. Arbet-Engels, A. Scherer, E. Yablonovitch, *Phys. Scr.* **1996**, T68, 17.
- [13] A. Vlad, A. Frölich, T. Zebrowski, C. A. Dutu, K. Busch, S. Melinte, M. Wegener, I. Huynen, *Adv. Funct. Mater.* **2013**, 23, 1164.
- [14] S. Matthias, F. Müller, C. Jamois, R. B. Wehrspohn, U. Gösele, *Adv. Mater.* **2004**, 16, 2166.
- [15] S. Venkataraman, G. J. Schneider, J. Murakowski, S. Shi, D. W. Prather, *Appl. Phys. Lett.* **2004**, 85, 2125.
- [16] H. Jansen, M. de Boer, R. Wiegerink, N. Tas, E. Smulders, C. Neagu, M. Elwenspoek, *Microelectron. Eng.* **1997**, 35, 45.
- [17] R. A. Gottscho, C. W. Jurgensen, D. J. Vitkavage, J. Vac. Sci. Technol., B: *Microelectron. Nanometer Struct.* **1992**, 10, 2133.
- [18] H. S. Sözüer, J. W. Haus, *J. Opt. Soc. Am. B* **1993**, 10, 296.
- [19] Y. Xia, B. Gates, Z. Y. Li, *Adv. Mater.* **2001**, 13, 409.
- [20] B. Chang, P. Leussink, F. Jensen, J. Hübner, H. Jansen, *Microelectron. Eng.* **2018**, 191, 77.
- [21] B. Chang, F. Jensen, J. Hübner, H. Jansen, *J. Micromech. Microeng.* **2018**, 28, 105012.
- [22] M. R. Gartia, Y. Chen, G. L. Liu, *Appl. Phys. Lett.* **2011**, 99, 151902.
- [23] C. L. Yu, H. Kim, N. de Leon, I. W. Frank, J. T. Robinson, M. McCutcheon, M. Liu, M. D. Lukin, M. Loncar, H. Park, *Nano Lett.* **2013**, 13, 248.
- [24] J. H. Choi, Y. S. No, J. P. So, J. M. Lee, K. H. Kim, M. S. Hwang, S. H. Kwon, H. G. Park, *Nat. Commun.* **2016**, 7, 11569.
- [25] K. A. Arpin, M. D. Losego, A. N. Cloud, H. Ning, J. Mallek, N. P. Sergeant, L. Zhu, Z. Yu, B. Kalanyan, G. N. Parsons, G. S. Girolami, J. R. Abelson, S. Fan, P. V. Braun, *Nat. Commun.* **2013**, 4, 2630.
- [26] N. Tétreault, G. von Freymann, M. Deubel, M. Hermatschweiler, F. Pérez-Willard, S. John, M. Wegener, G. A. Ozin, *Adv. Mater.* **2006**, 18, 457.
- [27] N. Muller, J. Haberko, C. Marichy, F. Scheffold, *Optica* **2017**, 4, 361.
- [28] P. V. Braun, S. A. Rinne, F. García-Santamaría, *Adv. Mater.* **2006**, 18, 2665.
- [29] R. Zhang, H. Ning, N. A. Krueger, D. Bacon-Brown, P. V. Braun, *Adv. Opt. Mater.* **2016**, 4, 1533.
- [30] E. Palacios-Lidón, J. F. Galisteo-López, B. H. Juárez, C. López, *Adv. Mater.* **2004**, 16, 341.
- [31] N. Tétreault, A. Mihi, H. Míguez, I. Rodríguez, G. A. Ozin, F. Meseguer, V. Kitaev, *Adv. Mater.* **2004**, 16, 346.
- [32] P. R. Villeneuve, S. Fan, J. D. Joannopoulos, *Phys. Rev. B* **1996**, 54, 7837.
- [33] J. D. Joannopoulos, S. G. Johnson, J. N. Winn, R. D. Meade, *Photonic Crystals: Molding the Flow of Light*, Princeton University Press, New Jersey **2011**.
- [34] S. Kim, A. N. Mitropoulos, J. D. Spitzberg, H. Tao, D. L. Kaplan, F. G. Omenetto, *Nat. Photonics* **2012**, 6, 818.
- [35] Y. Wang, D. Aurelio, W. Li, P. Tseng, Z. Zheng, M. Li, D. L. Kaplan, M. Liscidini, F. G. Omenetto, *Adv. Mater.* **2017**, 29, 1702769.